6th European Conference on Computational Mechanics (ECCM 6)
7th European Conference on Computational Fluid Dynamics (ECFD 7)
11 – 15 June 2018, Glasgow, UK

A FINITE VOLUME METHOD FOR HIGH MACH NUMBER FLOWS ON HO GRIDS

JEAN-MARIE LE GOUEZ[1]

[1]ONERA Aerodynamics, Aeroelasticity and Aeroacoustics Department
BP 80100 – Chemin de la Hunière FR-91123 Palaiseau Cedex
jean-marie.le_gouez@onera.fr https://www.onera.fr/en/staff/jean-marie-le-gouez

Key words: Finite Volume, unstructured grids, CFD, High-Order, k-exactness, Shocks.

Abstract. We present a spatially High Order cell-centered Finite Volume method based on a WLSQ reconstruction of the conservative variables or the components of the flux density tensor [1]. These reconstructed polynomials are projected on the cell interfaces to compute the fluxes. The weight distribution in the WLSQ permits to obtain a stable scheme without the need for a posteriori limiting the higher order derivatives of the reconstructed fields.

The face projected fields and their normal derivatives can then be associated with the most robust existing flux schemes [2], eventually dealing with discontinuous solutions for shock capturing.

Accurate expressions also of the wall boundary conditions enable to reach high grid convergence indices for transonic and supersonic flow computations around wing profiles.

The formulation could be extended to high order grids in a very CPU efficient way.

These novel features, in subsonic, transonic and supersonic situations, could be compared with the element-based spatially HO reference methods (DG, Flux Reconstruction, stabilized CG,…) and standard 2nd Order FV formulations, during the editions of the High Order CFD Workshop [3] and during Onera solver cross comparison projects.

1 INTRODUCTION

Stable and accurate flux integration methods on unstructured grids are needed for robust CFD solvers. In the context of cell-centered Finite Volume, the polynomial reconstruction of the fields of conserved or primitive variables over a wide source stencil by Least-Squares methods is the basis for a number of developments [3] [4] [5]. In the projection phase of the NXO numerical scheme, the reconstructed solution can be evaluated in a number of ways:

- at nodal face integration points, where dual-valued conservative variables from left and right-biased stencils serve as an input for an approximate Riemann solver,
- as a surface integral on these interfaces, for a single face evaluation of the fluxes from interface-averaged conservative variables,
- as a volume average of the field on some target cell in an overset grid problem.

This cell-centered Finite Volume method also makes use of an optional formulation where the reconstructed fields are not the conservative variables, but the components of the flux density tensor of each conservation equation. The flux tensor has a non-linear expression as

function of the conservative variables in all equations, except for the mass conservation. Its spatial reconstruction limits the overall asymptotic order of the scheme to 3, but it was shown in [1] that much higher grid convergence indices can be obtained with this scheme on grids of moderate refinement, and the entrance of the scheme into the asymptotic regime is obtained with a coefficient of the leading error term that is reduced by several orders of magnitude when compared to standard 2nd order FV methods.

The computations presented here use the flux density tensor reconstruction algorithm up to the fifth order, associated to a face-centered stencil and stabilized by first-order and eventually a blend of 1st- and 3rd-order grid difference operators across the interface, as in the JST scheme [2].

All coefficients of the linear combinations towards the interfaces are computed in the geometric preprocessor, they include an a priori stabilization feature that enhances the diagonal dominance of the overall scheme, by using fast decaying weights towards the periphery of the stencil, in the Weighted Least Square reconstruction.

This scheme was applied on high order grids made available at the 3rd and 4th HO CFD workshops, for the shock-free cases of the Ringleb flow and a subsonic bump [6].

Application examples dealing with supersonic and transonic flows around aerodynamic profiles are presented; they concern a Bow shock from a flow at Mach 4 encountering a flat plate with rounded edges, which is also a test case from the HO workshop, and Mach 0.8 and 0.95 flows around a NACA0012 profile.

For this last case the expression of the wall boundary condition was improved to interpolate within the wall stencils only over quantities that are more continuous across shocks. This enabled gains in accuracy in the wave drag exceeding 1 order of magnitude on the reference grids that were formerly used for studies with 2nd order FV solvers.

2 MAIN FEATURES OF THE SCHEME

2.1 High-order spatial integration of the fluxes over a curvilinear interface

Achieving a high space order in the Navier-Stokes schemes should permit to reduce drastically the number of cells in a grid to reach a target accuracy. At the walls in particular, it cells with curved boundaries must be used to represent properly the wall geometry.

With these grids that are still more refined in the wall normal direction in order to properly resolve the boundary layers, the curvature of the cell faces at the wall needs to be propagated inside the grid. A full formulation of the FV scheme on HO grids is found necessary, besides curved wall HO boundary conditions. In a first step, for the reconstruction itself, curvilinear integration is used for the volume integrals of the monomials that serve for the WLSQ.

The HO fluxes integration is then expressed in the following way, by introducing the components f, g, h of the inviscid and diffusive flux density tensors and the unit normal vector $\vec{\nu}(X, Y, Z)$ varying across the interface:

$$\frac{\partial W}{\partial t} + \frac{\partial (f_i - f_v)}{\partial x} + \frac{\partial (g_i - g_v)}{\partial y} + \frac{\partial (h_i - h_v)}{\partial z} = 0 \quad (1)$$

After integration on a cell of volume Ω enclosed in a discrete set of boundaries $\partial\Omega_n$, with the volume average of a field represented by an overbar and the surface average represented by an overhat,

$$\frac{\partial\left(\Omega\overline{W}\right)}{\partial t}+\sum_{n=1}^{ni}\oint_{\partial\Omega_n}\left(\vec{F}_i-\vec{F}_v-\vec{F}_{i,diss}\right).\ \vec{v}dS=0 \quad (2)$$

with $\vec{F}_i=\begin{bmatrix} f_i \\ g_i \\ h_i \end{bmatrix}$, $\vec{F}_v=\begin{bmatrix} f_v \\ g_v \\ h_v \end{bmatrix}$ the natural inviscid and diffusive fluxes, $\vec{F}_{i,diss}$ the added artificial dissipation, computed from the first and/or third order grid difference across the interface and discussed in the next section.

We compute in the preprocessor the array κ that relates the discrete fields in the stencil to the coefficients of the reconstructed polynomial [1]. Then we evaluate, component-wise and with the desired numerical accuracy, the face integral of the unit normal vector multiplied by the monomials of the base as $\oint_{\partial\Omega_n} X^i Y^j Z^k\ \vec{v}dS=\vec{\pi}_{\{ijk\}}$ (3).

The curvilinear flux integral is expressed as a linear combination over the stencil of the discrete components of the flux density tensor:

$$\begin{aligned}\oint_{\partial\Omega_n}\left(\vec{F}_i-\vec{F}_v\right).\ \vec{v}dS &= \sum_{c=1,nc}\vec{\pi}_{\{ijk\}}.\left[\kappa_{\{ijk\},c}(\hat{\vec{F}}_i-\hat{\vec{F}}_v)_c\right] \\ &= \sum_{c=1}^{nc}\left[\alpha_c\left(\bar{f}_i-\bar{f}_v\right)_c+\beta_c\left(\bar{g}_i-\bar{g}_v\right)_c+\gamma_c\left(\bar{h}_i-\bar{h}_v\right)_c\right] \end{aligned} \quad (4)$$

We need to store after the preprocessor, on each interface, the coefficients of the linear combinations α,β,γ, computed from the product of κ and $\vec{\pi}$, to obtain at a low CPU cost the flux curvilinear integrals for each equation of the NS system at each iteration of the solver.

2.2 Extension of the JST scheme at High Order on HO grids

We concentrate here on the inviscid fluxes of the governing equations. The scheme used is a centered scheme close to the JST scheme [2], with natural inviscid fluxes and an artificial dissipation with a shock detector. The 5 conservation equations in 3D are written:

$$\frac{\partial\left(\Omega\overline{W}_i\right)}{\partial t}+\sum_{n=1}^{ni}S_n\left(\hat{f}_{i,nat}-\hat{f}_{i,diss}\right)_n=0 \qquad i=1,5 \quad (5)$$

with $\overline{W}_i=\frac{1}{\Omega}\iiint_\Omega W_i dV$, $W=[\rho,\rho u,\rho v,\rho w,\rho e_t]^T$ and $\hat{f}_i=\frac{1}{S}\iint_S f_i dS$

- $\hat{f}_{i,nat} = \dfrac{\hat{f}_{i,left} + \hat{f}_{i,right}}{2} = \dfrac{\sum_{s\in St,left} \lambda_{left,s}\, \bar{f}_{i,s} + \sum_{s\in St,right} \lambda_{right,s}\, \bar{f}_{i,s}}{2}$ (6) is the mean of the reconstructed and face projected normal fluxes in the cells of the left and right stencil.
- $\hat{f}_{i,diss} = \varepsilon_2\, \omega \hat{\delta} W_i^* - \varepsilon_4 \omega \hat{\delta}\hat{\delta}\hat{\delta}\hat{\delta} W_i^*$ (7) is the artificial dissipation at high order, where W_i^* uses the total enthalpy rather than the total energy in the energy equation, $W^* = [\rho, \rho u, \rho v, \rho w, \rho h_t]^T$. $\hat{\delta} W_i^*$ is an evaluation at high order of the first grid normal difference of W_i^* over the interface and $\hat{\delta}\hat{\delta}\hat{\delta} W_i^*$ that of the third difference.

$\omega = \dfrac{|uS_x + vS_y|}{\sqrt{S_x^2 + S_y^2}} + a$ is the highest module of the eigenvalues of the flux Jacobian at the interface, computed from the stencil average of conservative variables, a the speed of sound.

The grid differences in the standard JST scheme are evaluated by a 2 point formula for the first difference and a 4 point formula for the third grid difference. The high order evaluations of the grid differences chosen here use the first and third normal derivatives of the reconstructed polynomials, which are polynomials in the coordinate normal to the interface, and of degrees k-1 and k-3.

The coefficients of these polynomials are multiples of those of the direct reconstruction ones, combined with the components of the unit normal vector $\nu = [\nu_X\ \nu_Y\ \nu_Z]^T$. All cells in the stencils are involved in the grid-normal difference formulas, which are linear interpolations over the whole stencil and extend naturally to arbitrary unstructured grids.

2.3 Improved wall boundary condition for transonic applications

A special processing is introduced in the stencils adjacent to the walls for transonic cases, in order to improve the quality of the reconstruction over the wall stencils containing the shock. In all wall stencils, we choose to reconstruct the spatial variation of the « lagrangian » fluxes, i.e. the projection of the flux density tensor components of each equation k on the unit vector in the direction of the velocity $\vec{U} = [u \quad v \quad w]^T$.

For each equation $\dfrac{\partial W_k}{\partial t} + \dfrac{\partial f_k}{\partial x} + \dfrac{\partial g_k}{\partial y} + \dfrac{\partial h_k}{\partial z} = 0$, we introduce $\varphi_k = \dfrac{f_k u + g_k v + h_k w}{\sqrt{u^2 + v^2 + w^2}}$ (8)

These fields, computed in all the cells of the wall stencils as shown on figure 1, hold a higher continuity over the shocks than the conservative variables or the face-normal fluxes (wall-normal here) used for the standard reconstructions presented before.

After computing through the “NXO extrapolation” the wall face average of the fields φ_k, there remains, in order to apply the wall b.c., to extract the pressure from these.

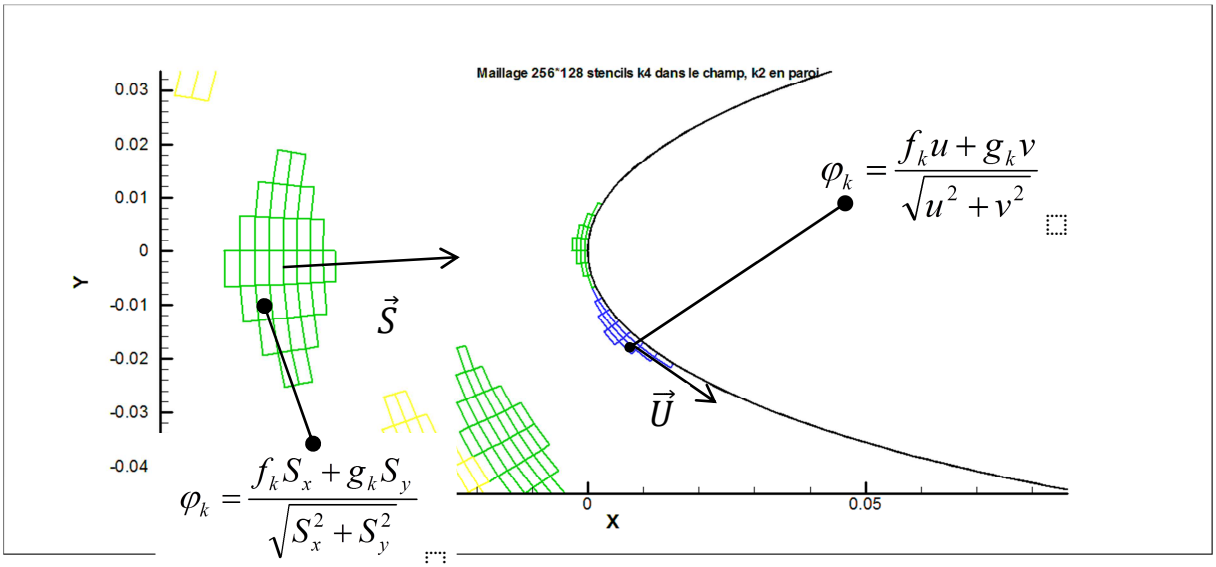

Figure 1: Reconstruction of flux densities in the direction of the global face normal or the local velocity vectors

The values φ_k are interpreted as the fluxes in the direction of the unit velocity vector at the wall $\vec{\tau} = (\tau_x, \tau_y, \tau_z)^t$. This vector is evaluated independently from the "NXO extrapolation" of the unit velocity vectors in the stencil; it is not imposed to be tangent to the wall. In order to solve for the wall pressure, this vector is also not imposed to be aligned with the wall velocity in the next equations (equation set (9) holds for any unit vector).

The quantities φ_k are related to the primitive variables by the following equations:

$$\varphi_1 = \rho(u\tau_x + v\tau_y + w\tau_z) = \rho u_\tau \quad \varphi_2 = \rho u_\tau u + p^* \tau_x \quad \varphi_3 = \rho u_\tau v + p^* \tau_y$$
$$\varphi_4 = \rho u_\tau w + p^* \tau_z \quad \varphi_5 = \rho u_\tau h_t \quad h_t = \frac{u^2+v^2+w^2}{2} + \frac{\gamma}{\gamma-1}\frac{p^*}{\rho} \qquad (9)$$

After eliminating ρ, u, v, w, h_t from these 6 equations, we obtain an equation of second degree for the pressure:

$$(\gamma+1)p^{*2} - 2p^*(\varphi_2\tau_x + \varphi_3\tau_y + \varphi_4\tau_z) + (\gamma-1)(2\varphi_5\varphi_1 - \varphi_2^2 - \varphi_3^2 - \varphi_4^2) = 0 \qquad (10)$$

This equation provides 2 roots that correspond respectively to a subsonic and a supersonic state. The selection between these is done from the direct extrapolation of the conservative variables to the wall to obtain the Mach number and express the compatibility relationship [6].

3 SHOCK-FREE VERIFICATION CASE OF A SMOOTH INVISCID BUMP

This 2D test case of a subsonic flow about a Gaussian shaped bump is provided by the High Order CFD workshop [7] with a series of 5 imposed quartic grids.

It was computed with the curvilinear reconstruction and integration scheme of section 2.1.

Three different degrees for the (k-exact) polynomial representation of the flux density tensor where used. The degree of reconstruction reduces in the stencils close to the boundaries from the one imposed in the center of the domain. These levels of accuracy were: k=1, which is close to an unlimited and really 2D MUSCL-type interpolation, k=2.25 (k=2 for 80% of the stencils and k=3 for 20%), k=3.15 (3 for 90% of the stencils and 4 for 10%).

The notion of "really 2D" refers to the fact that the reconstruction at any k order is a unique polynomial in all space coordinates over a cell-centered stencil, and the evaluation of this same polynomial is done at all the interfaces of the cell for upwind or centered schemes.

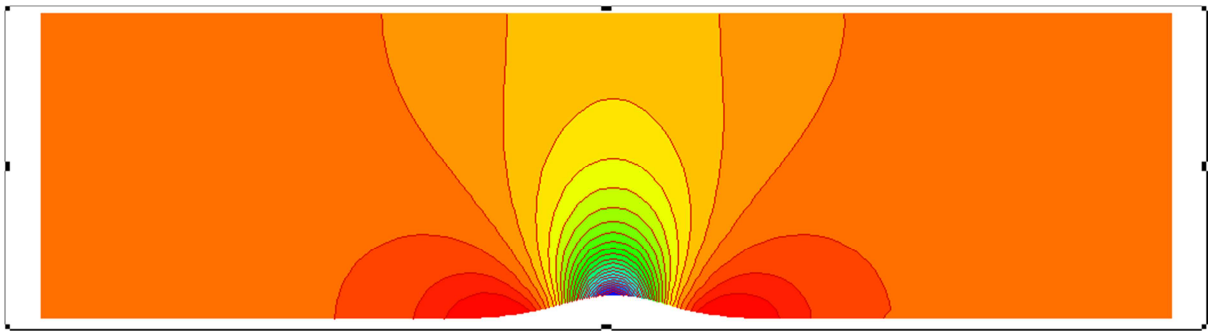

Figure 2: Field of density for the run on grid4: 3072 cells (= number of dof/equation)

The density field computed on grid 4 is shown on figure 2. Figure 3 presents the L2 norm of the entropy error over the grids, as a function of an average cell size. The grid convergence index reaches 4.1 for the k=3+ scheme, which is at par with the majority of the element-based solvers which contributed to this test case.

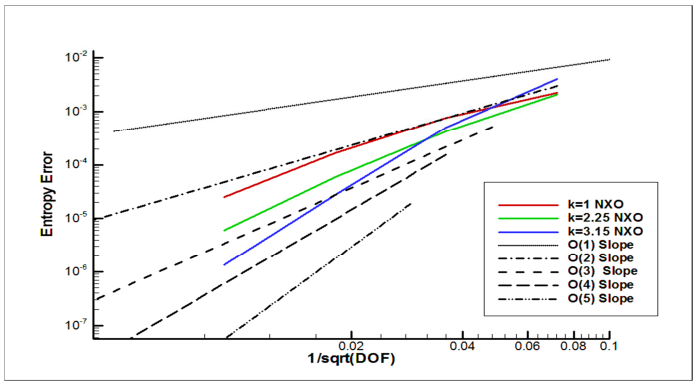

Figure 3: L2-norm of entropy error over the grids

4 SUPERSONIC VERIFICATION CASE FROM THE 5TH HO CFD WORKSHOP [8] (BOW SHOCK AT MACH 4)

This test case was to be computed on the 5 provided structured grids [8], adapted to the bow shock position for a reference 2nd order FV solver. In order to calibrate the amount of artificial dissipation and to compare it with the JST scheme [2], the scheme of section 2.2 was used on 1D stencils extending along the grid line normal to the interface. The only monomials of the base are powers of the normal coordinate.

The flow field and the coefficients of artificial dissipation are illustrated on figure 4.

The preprocessing is done successively with cell stencils of 5, 7 and 9 stencils enabling k-exact reconstructions from k2 to k5. The exact cell node coordinates are used, so varying size of the cells in the stencil is accounted for. The corresponding face stencils used for the artificial dissipation comprise 6, 8 or 10 cells, and enable to reconstruct k3 to k5 polynomials.

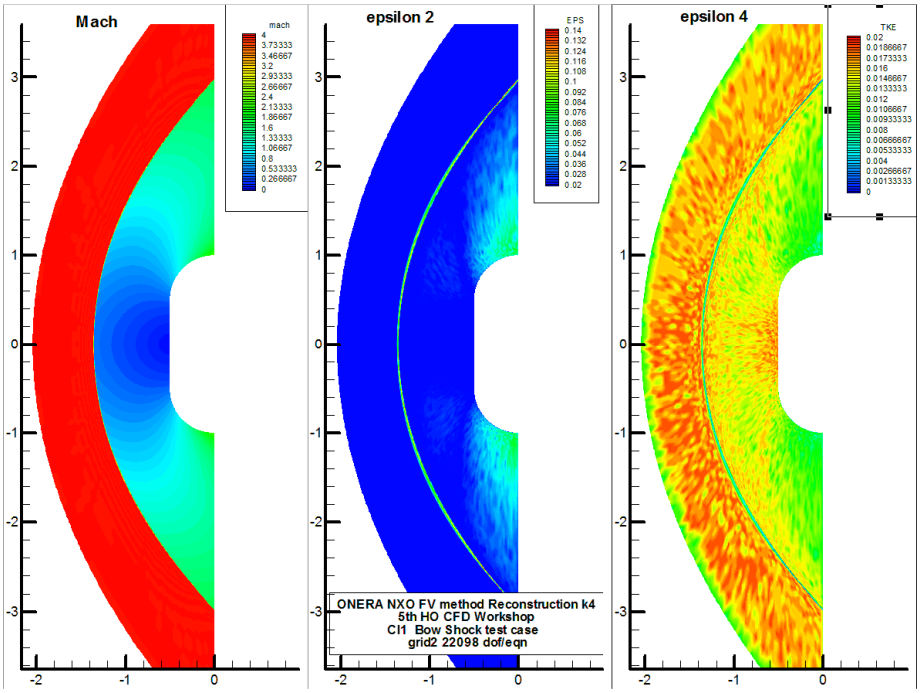

Figure 4: Fields of Mach number and coefficients of 2nd order and 4th order artificial dissipation (eqn. 7). Bow Shock at Mach 4, grid 2: 22098 dof/eqn

The main point that allows a higher accuracy is the stencil-reconstruction of face normal fluxes rather than conservative variables. These fluxes are continuous over the stencil across normal shocks when the grid is fitted to them.

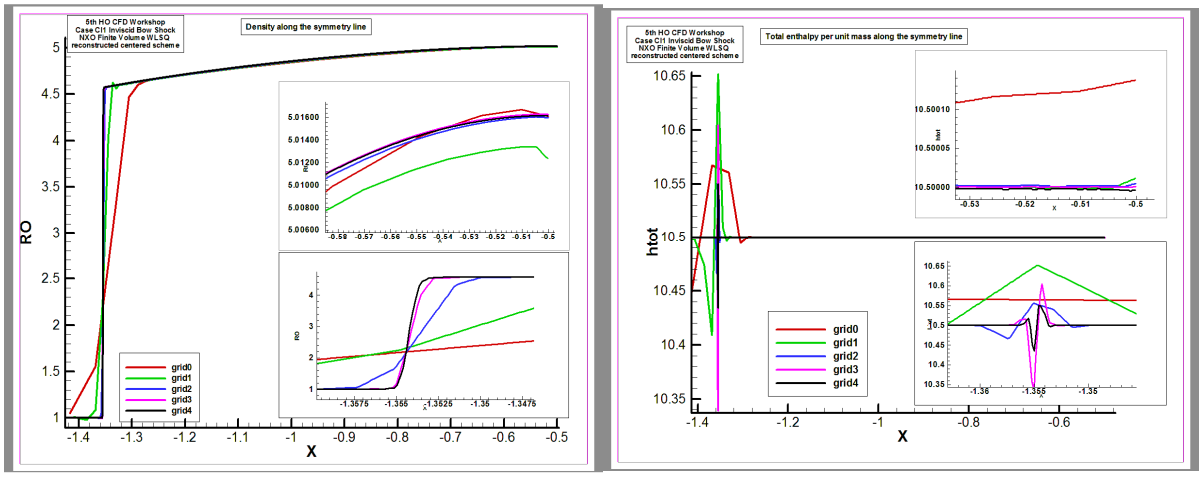

Figure 5 Bow shock: Density (left) and total enthalpy (right) on the symmetry axis Zooms at the stagnation point and at the shock region

On figure 5 is presented the evolution of the solution along the stagnation line, for the density and the total enthalpy. These illustrate the sharpness of the density jump capture and the convergence of the solution at the stagnation point.

The total enthalpy only departs from its reference value in 2 cells across the shock.

The relative error at the stagnation point for this quantity is of the order of 10^{-6} on all grids except for the coarsest one.

5 TRANSONIC VERIFICATION CASE (MACH 0.8 AND MACH 0.95 FLOWS AROUND A NACA0012 AIRFOIL)

Structured and unstructured grids are used. The NACA0012 profile was extended slightly after x=1 until it closes without modifying its equation. The NACA0012 profile was extended slightly after x=1 until it closes without modifying its equation.

The flow about a NACA0012 airfoil at Mach 0.8 without incidence is computed on a series of structured O-grids. These high quality grids that are not refined at the shock locations have been created by A. Jameson and J. Vassberg for their projects, in particular [10]. They were made available by them to ONERA for the projects of D. Destarac and his co-workers [11]. We acknowledge here their support and express our thanks.

These structured grids are interpreted as unstructured by the solver. Three successive options of the NXO scheme have been used, all with the reconstruction of normal components of the flux density tensor at all faces but the boundaries:

a/ The expression on linear grids, with wall slip boundary conditions processed by the HO extrapolation in the wall stencil of conservative variables,

b/ The same scheme at inner faces, and a wall boundary condition based on the reconstruction / extrapolation of “lagrangian” fluxes in the wall stencils and resolution of a second degree equation for pressure at the wall (section 2.3, eqn. 10),

c/ Same as b/, but with also a high order geometric representation of the wall face, as a quartic Lagrange polynomial in space, obtained by adding 3 supplementary definition points for the profile at their exact coordinates within each wall face.

Runs a/ were done on a series of grids of sizes from 128*128 to 1024*1024, which had previously been computed by a 2nd order cell-centred FV code at Onera.

The reconstruction k4 on a full 2d base was used in the field stencils, and k3 in the wall ones (comprising 25 cells in the field and 16 at the wall, see figure 1).

The field of absolute error on the total enthalpy field is plotted on figure 6 (reference value is 2.82). It is lower in the field than at the wall, with an error spot at the shock location.

We present on figure 7, as squares for the formulation a/, the absolute error in drag with a reference value Cx = 0.0083409 obtained from elsA with the JST scheme, and the relative error in total enthalpy at the wall, i.e. the contour integral along the profile of $\frac{\left|H_t - H_{t,\infty}\right|}{H_{t,\infty}}$.

The grid convergence index for the drag error is a little better than 3.5, while the one for the total enthalpy error is 1. The NXO solution on the finest grid is 0.00834083.

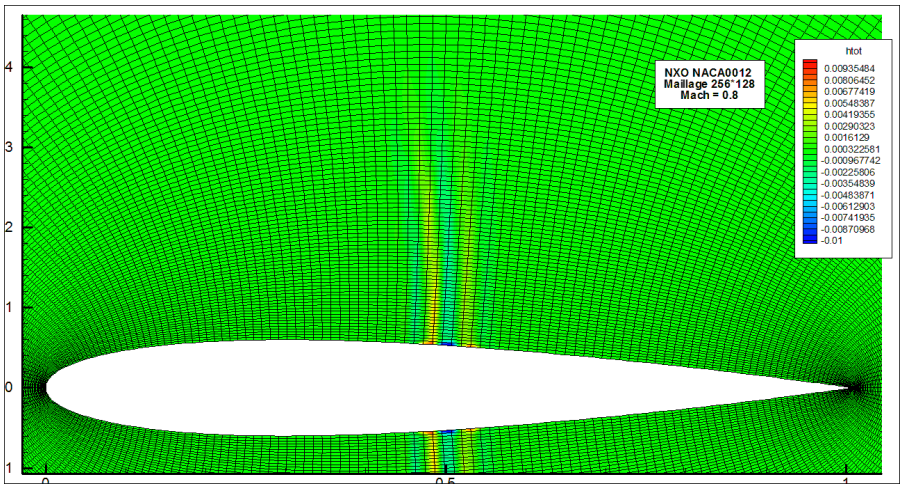

Figure 6: Field of total enthalpy absolute error for a grid 256*128 (tangential / normal) $H_{t,\infty}$ =2.82

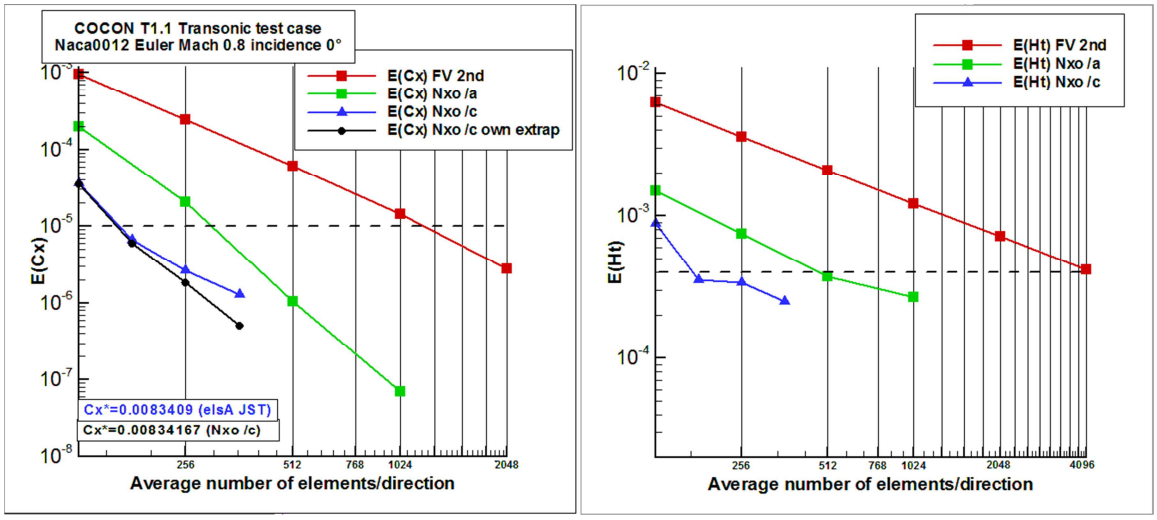

Figure 7: Error indices as function of the square root of the dof/eqn (average number of cells per direction) NXO results a/: green squares, c/: blue and black curves, grids 181*91, 256*128, 362*181, 512*256 of fig. 9

The solution with the most accurate wall boundary condition c/ is shown on figure 8.

We have plotted here, along both sides of the wall and with the cell index in abscissa, the 2 solutions of the equation of second degree for the wall pressure in green and blue, together with the one that was retained, in red, based on the evaluation of the Mach number.

The wall faces are numbered in clockwise order from the trailing edge. The stagnation point at center (i=128) is in the low subsonic zone, with a corresponding supersonic solution close to 0, then as we move downstream pressure decreases and the flow becomes supersonic.

It is noticeable that the pressure gradient along the wall is continuous where the flow becomes supersonic (i=105 and i=145), although we are changing the choice of the root of the second degree equation.

Then at the shock we switch again roots, without excessive wiggles near the shock.

The solution improvement, in drag and total enthalpy, is plotted on figure 7 as triangles and circles.

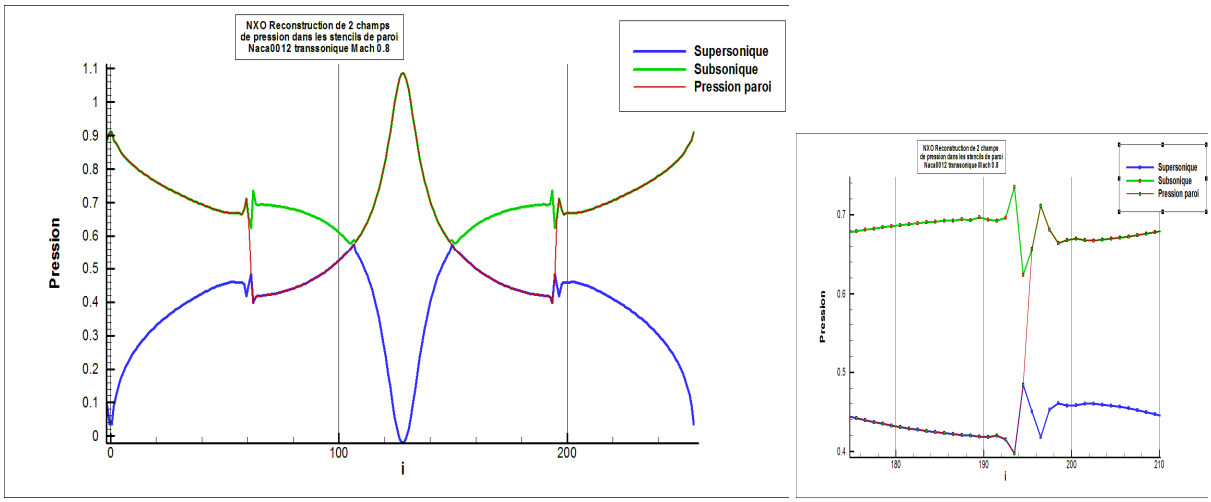

Figure 8: Solutions of the equation of 2nd degree. Wall pressure function of wall face index run c/ 256*128. Retained solution is in red; zoom at the shock location

For the curve with black circles, drag computed with the model c/ is extrapolated for an infinite fine grid to Cx*= 0.0083417 rather than the elsA value of 0.0083409 used before. The convergence rate for drag is 3.7, while the total enthalpy error stalls.

The total enthalpy field of run c/, on a grid of square cells, is plotted on figure 9a, with now a more continuous level of error inside the domain and at the wall.

Finally we present on figures 9b the error traces of the relative total enthalpy error, in log-scale, along the wall as function of the cell indices, for the 3 runs on the grid of figure 9a comprising 256*128 cells. Run a/ is in red, run b/ in green, and run c/ in blue.

The error levels of b/ and c/ are lower, except in the supersonic zone, between the cell faces 150 and 185, where the error in the initial model a/ drops near 10^{-6}. The b/ and c/ models are much more accurate across the shock and downstream it. The formulation with higher order geometry representation only improves the streamwise regularity of the solution.

The curvilinear integral of the relative error on total enthalpy on this grid is divided by a factor 3 from model a/ to model c/, 1.1 10^{-3} to 3.5 10^{-4}.

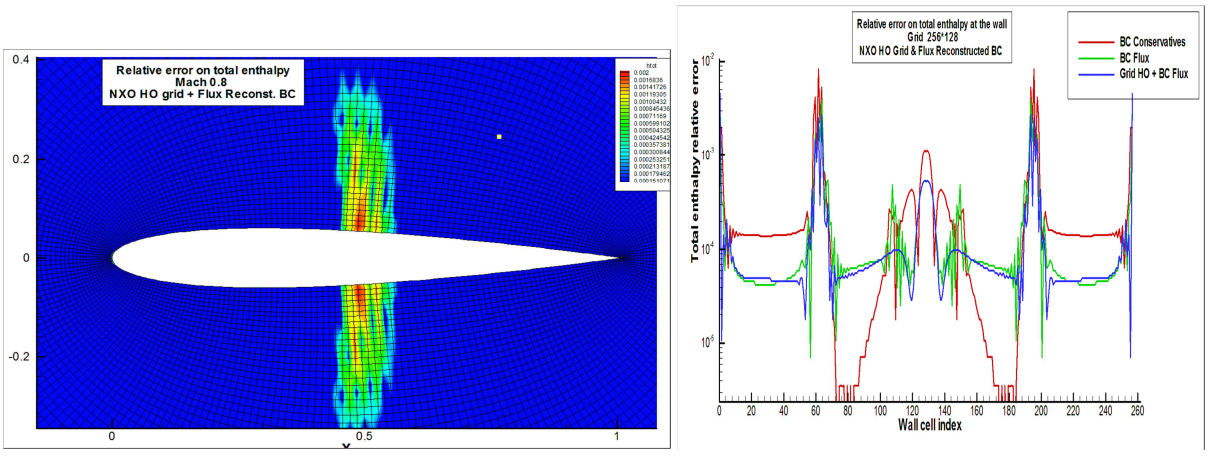

Figure 9: Run c/ 256*128. Relative error on total enthalpy in the field and at the wall: runs a,b, c/ 256*128

A second series of runs was performed on the same airfoil at Mach 0.95, with fully unstructured grids and stencils made of triangles. The formulation a/ was used, since the flow is supersonic along the wall, from 6% of chord, and gets subsonic way downwind.

The meshes used here stem from an Onera project with the hybrid (structured/ unstructured) version of elsA, where a goal-oriented grid adaptation method using the adjoint of the unstructured solver was developed [12]-[13].

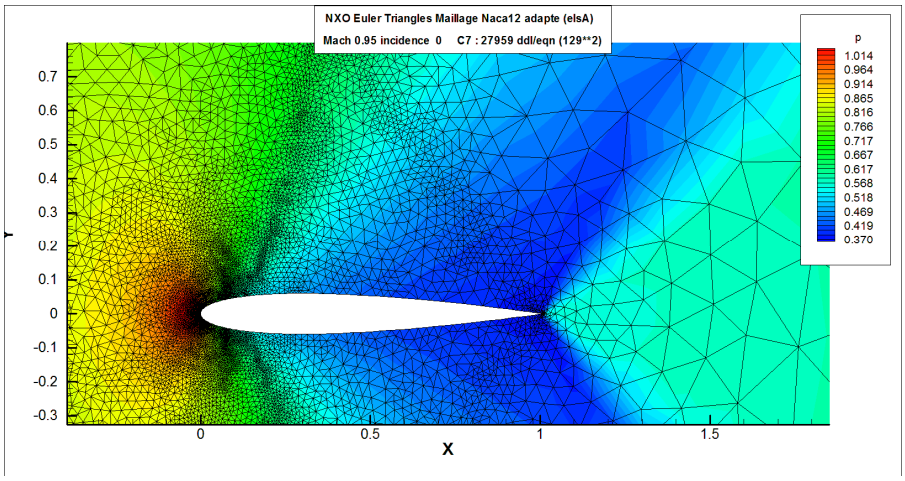

Figure 10: Pressure field for the NACA0012 transonic flow at Mach 0.95. Grid C2_7 27959 dof/eqn

Although the spatial schemes of elsA and NXO on unstructured grids strongly differ, the grid adaptation algorithm is also driven by the physics of the flow and the error decreases fast with the grid size. Figure 10 shows the grid refinement zones related to global flow features.

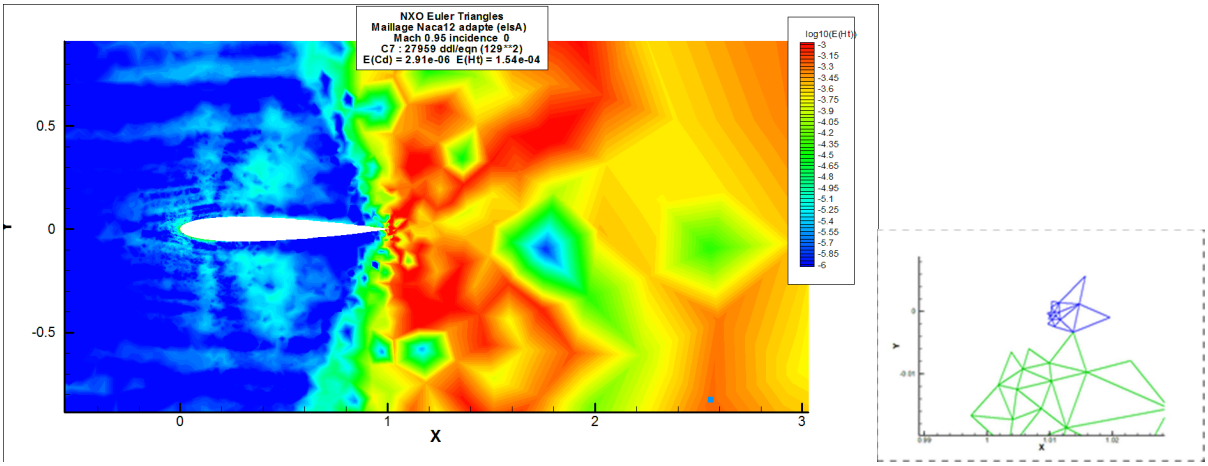

Figure 11: Grid C2_7. Relative total enthalpy error (log scale), NACA0012 transonic flow at Mach 0.95
Representation of some stencils near the airfoil downstream edge

The error field on figure 11 takes low levels along the profile. The errors as function of the mesh size are reported in table 1 and plotted on figure 12. High grid convergence rates are

evidenced on mid-size grids, owing to the grid adaptation algorithm. Errors in the wave drag below 10^{-5} are obtained with only 100^2 dof per equation.

The robustness and accuracy of the spatial scheme can be asserted, a full convergence of the residuals to machine accuracy is reached, despite the complex configuration of the 3rd_neighbour stencils in the refined zones shown on figure 11.

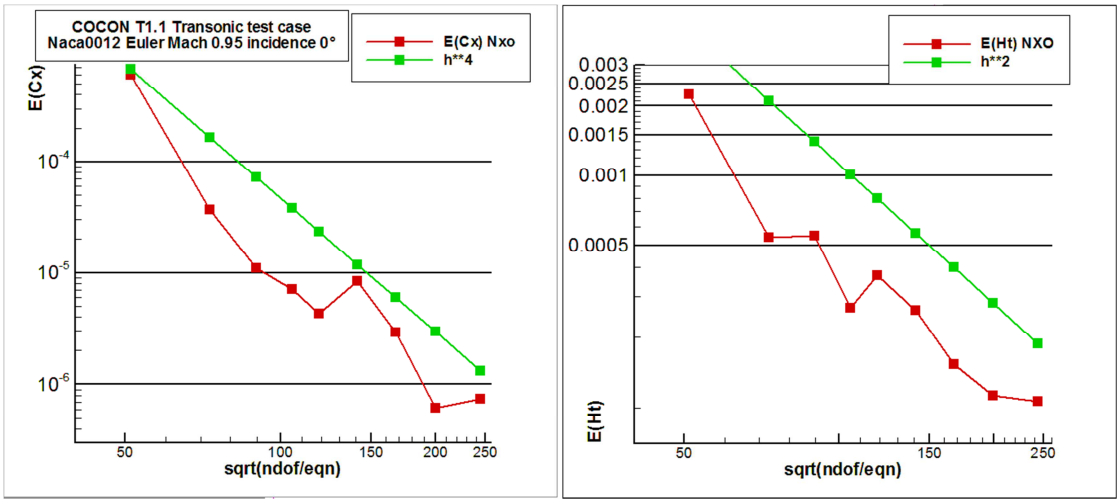

Figure 12: Error on the drag (reference value from the literature is 0.1097978)
Relative error in total enthalpy (log scale) NACA0012 transonic flow at Mach 0.95

Table 1: Results for computations on unstructured grids (automatically refined for the elsA Hybrid solver)

	Nb vertices	Nb triangles (dof/eqn)	Cd	E(Cd)	E(Ht)	Nit	Mem (MO)
C2_1	1352	2618 (51^2)	0.1103989	$6.0\ 10^{-4}$	$2.25\ 10^{-3}$	3700	47
C2_2	2738	5338 (73^2)	0.1098347	$3.7\ 10^{-5}$	$5.40\ 10^{-4}$	5050	50
C2_3	4092	8034 (90^2)	0.1097869	$1.1\ 10^{-5}$	$5.50\ 10^{-4}$	6050	56
C2_4	5640	11112 (105^2)	0.1098049	$7.1\ 10^{-6}$	$2.68\ 10^{-4}$	6300	78
C2_5	7146	14108 (119^2)	0.1098021	$4.3\ 10^{-6}$	$3.70\ 10^{-4}$	7500	99
C2_6	10049	19888 (141^2)	0.1098062	$8.4\ 10^{-6}$	$2.61\ 10^{-4}$	8900	140
C2_7	14100	27959 (167^2)	0.1098007	$2.9\ 10^{-6}$	$1.54\ 10^{-4}$	12500	195
C2_8	20000	39904 (200^2)	0.1097984	$6.2\ 10^{-7}$	$1.13\ 10^{-4}$	16200	275
C2_9	30000	59700 (244^2)	0.1097971	$7.5\ 10^{-7}$	$1.07\ 10^{-4}$	19300	420

6 CONCLUSION

The state of the art in spatially High Order Compressible CFD evolves rapidly [14]. The interpolation and flux integration phases of the NXO scheme provide robustness and accuracy on several types of coarse and optionally HO grids, on a wide range of Mach numbers.

Curved wall boundary conditions well adapted to the occurrence of flow discontinuities permit to enhance even further the quality of the results, on grids with low refinements that spatially high-order methods should demonstrate as relevant.

With this objective of strong algorithm efficiency on coarser grids, the asymptotic spatial order of the scheme becomes less salient.

7 REFERENCES

[1] J.M. Le Gouez, “High-Order Overset Interpolation via Weighted Least-Square Polynomial Reconstruction for Finite Volume CFD”, AIAA Paper 2016_2051, SciTech 2016, 4-8 Janvier 2016, San Diego, Californie.
[2] Antony Jameson. "Origins and Further Development of the Jameson–Schmidt–Turkel Scheme", AIAA Journal, Vol. 55, No. 5 (2017), pp. 1487-1510.
[3] T.J. Barth, Aspects of unstructured grids and finite-volume solvers for the Euler and Navier-Stokes equations, VKI lecture Series 1994-05,1995.
[4] S. Khohla et al. "Using Fourth order accurate spatial integration on unstructured meshes to reduce LES run times". AIAA 2008-782 , 46th AIAA Aerospace Sciences Meeting and Exhibit, January 2008, Reno, Nevada.
[5] Yoshiharu Tamaki, Taro Imamura, “A Novel Efficient Reconstruction Scheme for Unstructured Grids based on Iterative Least-Squares methods” SciTech 2016 San Diego, 54th AIAA Aerospace Sciences Meeting. 10.2514/6.2016-1100.
[6] J.M. Le Gouez, Researchgate project 2016
https://www.researchgate.net/project/NextFlow-Spatially-HO-Finite-Volume-method-for-Compressible-Navier-Stokes
[7] 3rd Workshop in High-Order CFD Methods. https://www.grc.nasa.gov/hiocfd/
[8] 5th International Workshop in High-Order CFD Methods.
https://how5.cenaero.be/content/presentations
[9] C.-W. Shu, S. Osher, Efficient implementation of essentially non-oscillatory shock-capturing schemes, J. Comput. Phys. 77 (1988) 439-471.
[10] Vassberg J, Jameson A. In poursuit of grid convergence, Part I: Two-dimensional Euler solutions. J of Aircraft 47(4) (2010) 1153–1166. 2010.
[11] Destarac D, Spurious Far-Field-Boundary Induced Drag in Two-Dimensional solutions. Journal of Aircraft 48(4) (2011) 1444-1455. 2011
[12] Jacques Peter, Maxime Nguyen-Dinh, Pierre Trontin. « Goal oriented mesh adaptation using total derivative of aerodynamic functions with respect to mesh coordinates - With applications to Euler flows” *Computers and Fluids*, Elsevier, 2012, 66, pp.194-214. 〈10.1016/j.compfluid.2012.06.016〉 . 〈hal-00769151〉
[13] Giovanni Todarello, Floris Vonck, Sébastien Bourasseau, Jacques Peter, Jean-Antoine Desideri. « Finite-volume goal-oriented mesh adaptation for aerodynamics using functional derivative with respect to nodal coordinates”. Journal of Computational Physics, Elsevier, 2016, 313, pp.21.<10.1016/j.jcp.2016.02.063> <hal-01410153>
[14] Z.J. Wang, K.J. Fidkowski, R. Abgrall, F. Bassi, D. Caraeni, A. Cary, H. Deconinck, R. Hartmann, K. Hillewaert, H.T. Huynh, N. Kroll, G. May, P-O. Persson, B. van Leer, and M. Visbal “High-Order CFD Methods: Current Status and Perspective,” International Journal for Numerical Methods in Fluids, 72, 811-845, (2013).